Single-Molecule Magnet Behavior and Spin Structure of an Fe^{III}_7 Cartwheel Cluster Revealed by Sub-Kelvin Magnetometry and Mössbauer Spectroscopy: The Final Pieces of the Puzzle

Juan Bartolomé,* Elena Bartolomé, Fernando Luis, Enrique Burzurí, Agustin Camón, George Filoti, Ayuk M. Ako, Jonas Braun, Valeriu Mereacre, Christopher E. Anson, and Annie K. Powell*

ABSTRACT: The spin frustration and other magnetic properties of the "cartwheel" heptanuclear cluster $[Fe^{III}_7O_3(O_2C^tBu)_9(Me\text{-}dea)_3(H_2O)_3]$ (Me-deaH$_2$ = *N*-methyldiethanolamine) have been previously investigated; we present here a Mössbauer spectroscopic study and sub-Kelvin magnetization and ac susceptibility measurements which enable a complete magnetic picture of this frustrated cluster. ^{57}Fe Mössbauer spectra above 150 K showed three doublets in a 1:3:3 ratio, which could be assigned by their respective quadrupole splittings to the central Fe(1) and the peripheral Fe(2) and Fe(3). The field dependence of the corresponding magnetic sextets at 3 K showed that the spins on the central Fe(1) and the three peripheral Fe(2) sites with O_5N coordination are oriented mutually coparallel, while these are antiparallel to the spins on the peripheral Fe(3) sites with O_6 coordination, resulting in an overall $S = 5/2$ ground state. This provides experimental confirmation of the previously proposed spin ground state structure. Upon cooling to sub-Kelvin temperatures, a crossover to spin blocking with $T_B \approx 0.21$ K could be observed. This single-molecule magnet behavior had been expected but had not been observable with a conventional SQUID. The anisotropy barrier, of 3-fold symmetry, can be described in terms of the parameter $D/k_B = -0.47$ K and a fourth-order perturbation; the latter enables thermally activated quantum tunneling through the excited sublevel $m_z = \pm 3/2$, with an activation barrier of $U/k_B = 1.9$ K.

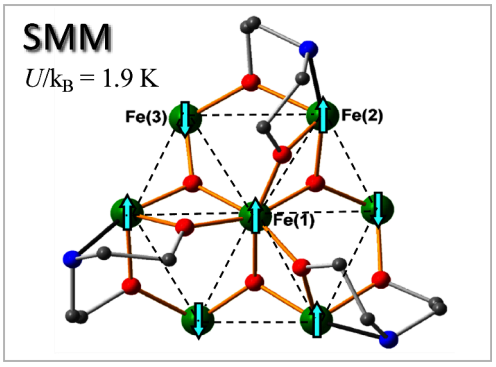

INTRODUCTION

Cyclic complexes have been of particular interest as models of one-dimensional chain compounds and in the study of quantum-size effects.[1] A particularly interesting class is the so-called molecular ferric wheels with nuclearity Fe_n ranging from 6 to 36 Fe^{III} ions.[2−13] The magnetization of the ferric wheels exhibits step-like field dependencies at low temperatures due to the importance of finite-size quantum effects.[14−17] Initially, these systems were regarded as ideal models for the finite-size version of the linear 1D Heisenberg chain, but subsequently, it was realized that their magnetic behavior at low temperatures is best described by a quantized rotation of the Néel vector and, hence, is more similar to that of 2D and 3D materials.[18−20] Moreover, quantum phenomena such as Néel-vector tunneling were demonstrated.[21] Because of the rich physics observed in molecular wheels and a promising potential for quantum computing,[22,23] this class of molecules has become increasingly important.

Ethanolamine ligands have been employed extensively in the construction of a variety of wheel-shaped complexes some of which have shown single-molecule magnet (SMM) properties.[10,24,25] The group of Saalfrank developed the use of diethanolamine-based ligands to create cyclic six and eight-membered Fe rings with a central templating alkali metal ion which is akin to the axle of a cartwheel.[7] Replacing this central diamagnetic templating ion with Fe^{III} switches on spin frustration effects.[26−33]

TEST BEDS FOR SPIN FRUSTRATION

Over the last three decades, the concept of spin frustration has been defined in different ways, at least partly depending on the background of the researcher and the nature of the frustrated system.[34] The strict definition of Kahn, preferred by physicists, states that a frustrated polynuclear system has a degenerate ground spin state.[35] Schnack proposed a similar but broader version of this, in which a frustrated spin system is one that cannot be described as bipartite.[34] In contrast to this is the more simplistic concept, described by Christou's group as "most useful to molecular chemists", in which a polynuclear system is unable to adopt any simple Ising-like "spin-up/spin-

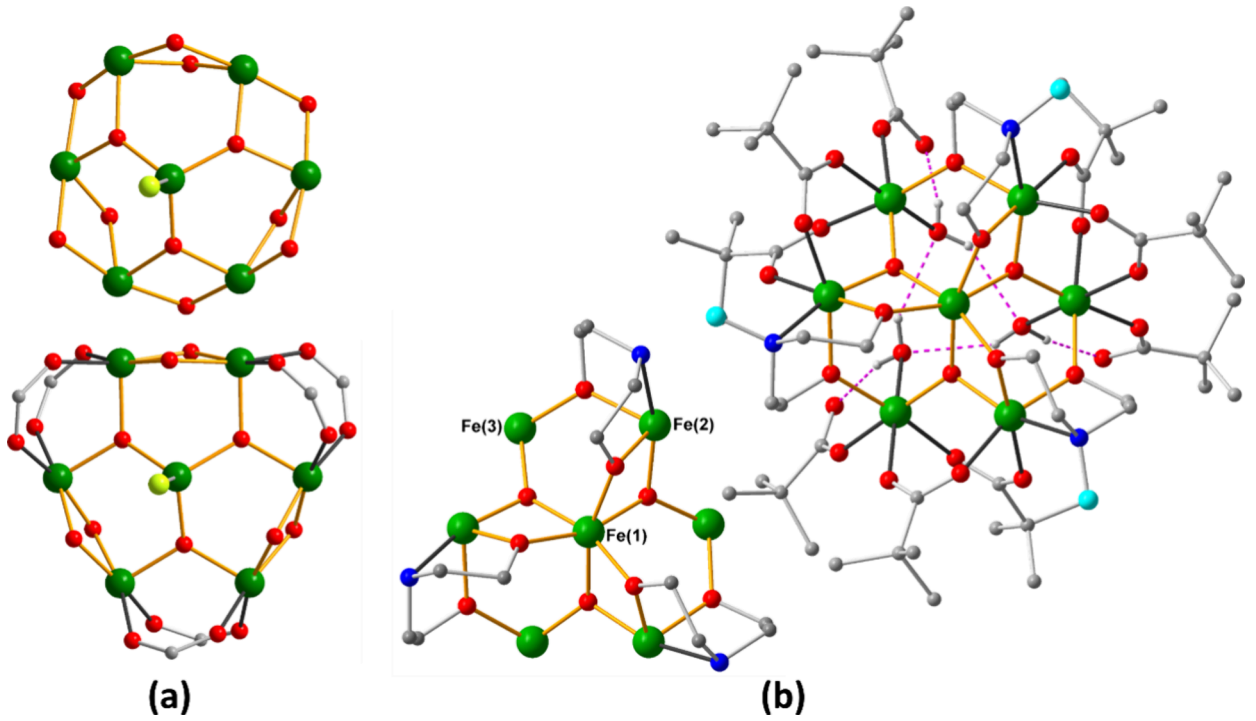

Figure 1. (a) Cores of Fe^{III}_7 clusters in which the central tetrahedral Fe^{III} is linked to the remaining six by three $(\mu_3\text{-}O)^{2-}$ bridges,[29−31,33] the doubly bridging oxygens are either alkoxido or hydroxido. (b) Core and molecular structure of the clusters $[Fe^{III}_7(\mu_3\text{-}O)_3(R\text{-}dea)_3(piv)_9(OH_2)_3]$ (R = −Me,[32] **1a**; $-CH_2CH_2OH$,[26,27] **1b**; $-CH_2CH(Me)OH$,[26] **1c**; $-Bu^n$,[27] **1d**; −Ph,[27] **1e**). Color code: Fe, green; O, red; N, blue; C, gray; H, white; R, cyan; organic H atoms omitted for clarity.

down" spin structure in which the relative orientations of the spins on each pair of coupled ions is consistent with the sign of the respective coupling between them.[36,37] More recently, Winpenny's group have reviewed both definitions and proposed the adoption of three categories of frustration, in which their Type I corresponds to the Kahn definition, while Types II and III involve systems more aligned with the "molecular chemists'" approach.[38] Specifically, their Type II systems have a spin ground state lower than that achievable with simple parallel and antiparallel classical spins, while Type III systems have a ground state in which a spin structure that can be described in terms of a "spin up/spin down" coexists with competing antiferromagnetic interactions.

Within Fe^{III} chemistry, the triangular "basic carboxylate" coordination clusters $[Fe^{III}(\mu_3\text{-}O)(O_2CR)_6(L)_3]^+$ proved an early test-bed for studies on spin frustration, since the three $S = 5/2$ spins involved are unable to adopt any simple Ising-like "spin-up/spin-down" spin structure consistent with all three antiferromagnetic Fe−Fe couplings. Indeed, such compounds are often drawn with a "spin-up/spin-down/spin-up" structure, which generally results in an overall $S = 1/2$ ground state spin[39] corresponding to Type II frustration.

The next step up involves systems built up from edge-sharing Fe^{III}_3 triangles. Here, the study of Fe^{III}_7 clusters in which a central Fe^{III} is surrounded by a hexagonal ring of six further such ions has proved particularly fruitful for a number of reasons. First, the planar spin topology with its 3-fold symmetry allows the number of distinct coupling constants J to be kept to a manageable number (four, or fewer if comparable couplings can be grouped). Second, such systems are closely analogous to an $S = 5/2$ Heisenberg star, one of the few frustrated spin systems which can be solved exactly.[40,41] Finally, the structures of many higher-nuclearity Fe^{III} coordination clusters can be viewed as having a central Fe^{III}_7 core, with the remainder of the cluster being extended from the rim of this core.[42−44] or built onto a face of the disc.[33,45] Some polynuclear Fe(III) clusters can be envisaged as small versions of double hydroxide clay type structures related to brucite, as in Fe_{17} and Fe_{19} clusters described in ref 42. Understanding the possible spin structures of these Fe_7 subunits can then prove crucial to the rationalization of the overall spin structure and the often high ground state spin of these larger clusters.[33,43,46−50]

In contrast to the triangular $Fe^{III}_3(\mu_3\text{-}O)$ systems, where the spin frustration generally results in the minimum possible $S = 1/2$ spin ground state, it has been previously shown that in higher-nuclearity clusters such as the Fe^{III}_7 clusters described in the previous paragraph the spin frustration can result in rather large spin ground states.[27,29] Such Fe^{III}_7 systems can, in theory at least, adopt spin ground states $S = (2n + 1)/2$ ranging from 1/2 up to 35/2, depending on the signs and relative magnitudes of the various coupling constants. However, since with Fe^{III} we are dealing almost exclusively with antiferromagnetic interactions the realistic maximum for S is 25/2, with parallel 5/2 spins on the six outer ring Fe^{III} ions and an antiparallel 5/2 spin on the central Fe^{III} axle. This would be the case if the couplings between the central Fe^{III} and those in the surrounding ring are much more strongly antiferromagnetic than those between the six Fe^{III} ions in the ring.

The coupling scheme in a group of clusters, in which a central Fe^{III} with a tetrahedral geometry is linked via three $(\mu_3\text{-}O)^{2-}$ oxido bridges to the outer six Fe^{III}, which are then bridged by a combination of alkoxido and carboxylato bridges (Figure 1a) approaches this situation. The overall spin ground state of these clusters was found to depend critically on the nature of the bridging ligands around the outer ring. This tunes

the Fe−oxo−Fe angles and hence the magnetic coupling constants J. For this reason, a wide range of ground states, S = 7/2 or 9/2, 15/2, and 21/2, has been reported for such clusters.[29−31,33] The latter value approaches the 25/2 limit mentioned earlier, but without reaching it. As such they do not fit the Type II or III spin frustration categories proposed in Baker et al.,[38] and are best categorized as Type I.

By contrast, the family of clusters (Figure 1b) with formula $[Fe^{III}_7(\mu_3\text{-}O)_3(\text{R-dea})_3(\text{piv})_9(OH_2)_3]$, where $(\text{R-dea})^{2-}$ corresponds to a doubly deprotonated *N*-substituted diethanolamine or triethanolamine ligand (R = Me,[32] **1a**; R = $-CH_2CH_2OH$,[26,27] **1b**; R = $-CH_2CH(Me)OH$,[26] **1c**; R = $-Bu^n$,[27] **1d**; R = −Ph,[27] **1e**) all have a well-defined ground state with S = 5/2, and thus are categorized as showing Type III frustration. A series of papers has focused on how the interplay of the antiferromagnetic couplings within these clusters gives rise to such a ground state, and on the relative orientations of the spins on the constituent Fe^{III} centers within that ground state, and the work presented here on the methyl analogue **1a** completes this study. It is therefore convenient to summarize the previous work here.

In 2006, Jones et al. reported the structures and magnetic properties of the clusters **1b** and **1c** from this series.[26] Magnetization and susceptibility measurements gave very similar results for the two compounds, and indicated S = 5/2 spin ground states, while powder X-band electron paramagnetic resonance (EPR) measurements on **1b** yielded values of D = +0.28 cm^{-1} and E/D = 0.21, although they stated that even these parameters did not simulate the data well. Indeed, one can note that a powder X-band measurement will lead to almost complete overlap of the expected signals.

The following year, some of us reported the structures of the hydroxyethyl, *n*-butyl, and phenyl analogues **1b**, **1d**, and **1e**, and confirmed the S = 5/2 ground state.[27] However, SQUID measurements on an orientated single crystal of the butyl analogue **1d** showed unequivocally that D < 0, with these Fe^{III}_7 clusters having easy-axis anisotropy, and a value of D = −0.30(2) cm^{-1}, i.e., the same magnitude but the opposite sign compared to the value found in ref 26, was obtained. It was also noted that the large E/D ratio found in ref 26 was inconsistent with the C_3 symmetry of the molecules, for which one would expect E = 0, and it was suggested that single-crystal EPR measurements might clarify the situation.

Single-crystal high frequency- electron paramagnetic resonance (HF-EPR) measurements on the analogous cluster with R = Me, **1a**, were indeed published by Datta et al.[51] These confirmed the uniaxial easy-axis nature of the cluster, since that the five peaks all increased in intensity with increasing applied field. A value of D = −0.36 cm^{-1} was obtained and the data could be fitted well without the need for an E parameter. The cluster was thus described as an SMM, even though no slow relaxation effects had been experimentally observed. It was also noted that the HF-EPR spectra showed three weak peaks, in addition to the five corresponding to the S = 5/2 ground state. Several possible explanations for these were suggested, including the presence of a low-lying excited state with S = 3/2. However, it was noted that no such low-lying state is to be expected in this system and density functional theory (DFT calculations on the isostructural analogue, in which the pivalate ligands had been replaced by benzoates, showed that the first excited state has S = 7/2 and is 157 cm^{-1} above the S = 5/2 ground state.[33]

In 2022, Hale et al. reported[32] the crystal structure of compound **1a**, which was found to crystallize in the trigonal space group *R*3 with the cluster molecule having 3-fold site symmetry. However, one should note the possibility of a symmetry-breaking phase transition between 173 K (the temperature of their structural determination) and the much lower temperatures of the EPR and magnetization measurements. They also made a detailed analysis of the antiferromagnetic couplings within the cluster core, which they determined both from their magnetostructural correlation[32,52] and by broken-symmetry DFT calculations (for their coupling constants, see S1). Both methods gave similar coupling constants and both sets of couplings gave simulated susceptibilities and magnetizations in good agreement with the experimental data. Once again a well-isolated S = 5/2 ground state was confirmed. From the coupling constants this was rationalized in terms of parallel S = 5/2 single ion spins on the central Fe^{III} and on the three outer Fe^{III} to which the Me-dea nitrogen atoms are coordinated with the spins on the other three outer Fe^{III} (those with O_6 coordination environments) oriented antiparallel. It was briefly mentioned that no χ''_M signal could be observed. A second paper reported a similar dual magnetoelastic correlations/density functional theory-(MSC/DFT) approach to the analogous cluster to **1a** but with benzoate instead of pivalate as the carboxylate ligand, with similar conclusions being drawn.[33]

In this paper, we report what could be considered to be the final pieces of the jigsaw puzzle that is the $[Fe^{III}_7(\mu_3\text{-}O)_3(\text{R-dea})_3(\text{piv})_9(OH_2)_3]$ family of coordination clusters. We present a variable-field ^{57}Fe Mössbauer spectroscopic study of compound **1a**, which gives experimental confirmation of the spin structure deduced by Hale et al.,[32] together with sub-Kelvin ac susceptibility and single-crystal magnetization measurements that show experimentally that this compound is indeed an SMM, albeit one with a blocking temperature of only 0.21 K. We also show that the three weak peaks observed by Datta et al.[51] in the HF-EPR spectrum of **1a** can indeed be explained in terms of a low-lying excited state, but an m_z = 3/2 sublevel of the ground state rather than an excited state with S = 3/2.

EXPERIMENTAL SECTION

Synthesis of $[Fe^{III}_7O_3(O_2C^tBu)_9(\text{Me-dea})_3(H_2O)_3]$ (1a). Our synthesis of **1a** is given here as it differs from that of Hale et al.[32] All reagents were obtained from commercial sources and were used as received, without further purification. All reactions were carried out under aerobic conditions. The elemental analyses (CHN) were performed using an Elementar Vario EL analyzer. Fourier transform IR spectra were measured on a PerkinElmer Spectrum One spectrometer with samples prepared as KBr pellets.

To a stirred mixture of $[Ni_2(\mu\text{-}OH_2)(O_2CCMe_3)_4(HO_2\text{-}CCMe_3)_4]$ (0.09 g, 0.10 mmol) and $[Fe_3O(O_2CCMe_3)_6](O_2CCMe_3)$ (0.10 g, 0.10 mmol) in MeCN (20 mL) was gradually added a solution of *N*-methyldiethanolamine (2.00 mmol) in MeCN (5 mL). The presence of Ni(II) gives rise to a very pure Fe(III) only product, as was shown earlier in ref 27. The resulting mixture was stirred at ambient temperature for 2 h, filtered and allowed to evaporate. Small needle-like crystals of cluster **1a** were obtained after 24 h, collected by filtration, washed with acetonitrile and dried under vacuum. Yield: 41 mg, 54% based on Fe. Calculated (found) for $C_{60}H_{120}Fe_7N_3O_{30}$: C 41.07 (41.10), H 6.89 (6.77), N 2.39 (2.63). Selected IR data (KBR disk cm^{-1}): IR (KBr [cm^{-1}]): 423 (w), 482 (w), 528 (m), 580 (s), 603 (m), 684 (m), 761 (vw), 785 (w), 879 (w), 902 (w), 1000 (m), 1029 (m), 1059 (w), 1102 (m), 1144 (vw), 1227 (s), 1262 (vw), 1287 (vw), 1357 (s), 1370 (s), 1408 (s), 1422 (vs), 1459 (m), 1483

(vs), 1571 (vs), 2812 (w), 2867 (s), 2901 (s), 2926 (s), 2959 (s), 3499 (m, br).

Crystallography. Data were collected at 100 K on a Bruker SMART Apex CCD diffractometer using graphite-monochromated Mo Kα radiation. Semiempirical absorption corrections were made using SADABS.[53] The structure was solved by direct methods using SHELXS,[54] followed by full-matrix least-squares refinement against F^2 (all data) using SHELXL-97[54] and SHELXL-2019/3.[55]

Anisotropic refinement was used for all ordered non-H atoms; organic H atoms were placed in calculated positions, while coordinates of hydroxo H atoms were refined. The refinement allowed for the presence of both merohedral and inversion twinning. Crystallographic information and refinement details are summarized in Table S1. Our crystal structure, measured at 100 K, is essentially identical to the structure determined at 173 K and published by Hale et al.[32] Note that in ref 32 the CCDC deposition number for the Hale structure was accidentally omitted; it is CCDC 2164410. To avoid duplication in the database, our CIF file has not been deposited but can be found in the Supporting Information to the present paper.

Magnetic and Mössbauer Measurements. Magnetic measurements were conducted on immobilized powder samples using a SQUID MPMS-5S. Susceptibility data were collected over a temperature range of 1.8 and 300 K under applied magnetic fields of 1 and 10 kOe. Additionally, magnetization isotherms were measured up to 50 kOe at temperatures ranging from 1.8 to 8 K. The magnetization measurements for the powdered sample of **1a** (see Figures S1 and S2) were in good agreement with data previously reported by Hale et al.[32] thus confirming the identity and purity of our sample.

In addition, low-temperature magnetization measurements at T = 0.38, 0.78, and 1.2 K were performed on a single crystal using a MicroHall magnetometer. The sensor consists of a GaAs/GaAsAl heterostructure, which generates a bidimensional electron gas, and is designed with two in-line crosses of 200 × 200 μm^2. A needle-shaped single crystal, with dimensions of 1.47 × 0.23 × 0.23 mm (0.08 mm^3, 1.0 × 10^{-4} g), was fixed with vacuum grease on one sensor cross and oriented with the c-axis aligned along the direction of the applied magnetic field. The field is applied parallel to the sensor plane. The signal from the bare cross is subtracted from the sample signal with a lock-in differential amplifier. The input current was I = 20 μA to avoid any heating of the sample at low temperatures. The sensor was in thermal contact with the cold finger of a ^{3}He refrigerator, and the temperature was automatically controlled. The sensitivity of the microHall sensor magnetometer is 10^{-10} emu.[56]

Ac susceptibility measurements in the very low temperature range of 0.1−3 K were performed on a powder sample using a susceptometer implemented in a ^{3}He−^{4}He cryostat. The excitation field was set at h_{ac} = 120 mOe, and the frequencies used were f = 0.133, 0.333, 1.333, and 13.33 kHz. The data in the overlap region with the SQUID ac susceptibility measurements were used to convert the low temperature data from arbitrary units to absolute units.

Mössbauer spectra (MS) were acquired using a conventional spectrometer in constant-acceleration mode, equipped with a ^{57}Co source (3.7 GBq) in rhodium matrix. Isomer shifts are given relative to α-Fe at room temperature. The sample was placed inside an Oxford Instruments Mössbauer-Spectromag 4000 Cryostat, which has a split-pair superconducting magnet system for applied magnetic fields up to 70 kOe. These fields are oriented parallel to the sample holder and perpendicular to the γ-ray direction. The sample temperature can be varied between 3 and 300 K. The fitting of the spectra and parameter optimization were performed using the NORMOS program.[57,58]

RESULTS AND DISCUSSION

Synthesis and Structure. Compound **1a** was obtained in high yield using a different method from that previously reported by Datta[51] and Hale.[32] The structure of **1a** has been previously described,[32] but it is briefly described here to aid in the understanding of the magnetic results and has similarities with previously reported related clusters.[26,27,51]

Compound **1a** crystallizes in the trigonal space group $R\bar{3}$, and occupies a site with crystallographic 3-fold symmetry. The molecular structure and cluster core are shown in Figure 1b. The core topology consists of an outer ring of six peripheral Fe^{III} which are each linked to a central Fe^{III}, which can be described as a cartwheel with the central Fe^{III} representing the axle of the wheel. The structure of **1a** consists of an [Fe$^{III}_7$(μ_3-O)$_3$]$^{15+}$ core, with the peripheral ligation provided by six μ_2-bridging pivalate ligands and three chelating-bridging (Medea)$^{2-}$ ligands, with three terminal unidentate pivalate ligands and three H_2O ligands coordinated to Fe(3) and its symmetry equivalents. Three types of Fe^{III} centers can thus be distinguished based on their coordination environments.

Static Magnetic Properties. The magnetization $M(H)$ curves measured at T = 0.38, 0.78, and 1.2 K on a single crystal of **1a** are shown in Figure 2, together with the isotropic S = 5/2

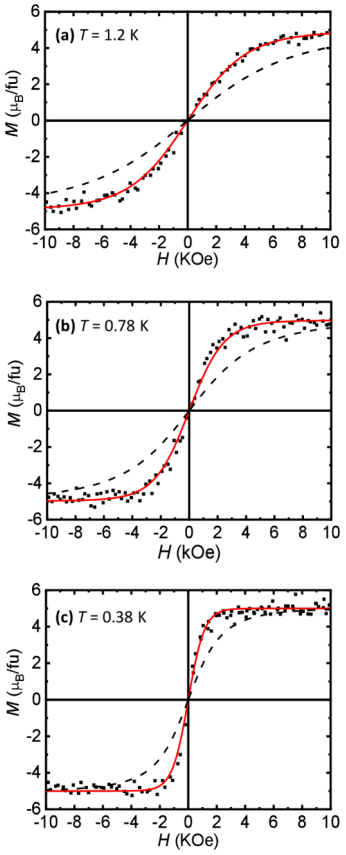

Figure 2. Magnetization as a function of the applied magnetic field, $M(H)$, for **1a** with the field parallel to the c-axis measured on a single crystal using a microHall magnetometer at (a) T = 1.2 K, (b) T = 0.78 K, and (c) T = 0.38 K. Solid red lines: simulations for uniaxial S = 5/2, with cluster crystal-field anisotropy parameter D/k_B = −0.47 K and g = 2. Dashed black lines: Brillouin function for S = 5/2. "fu" = formula unit.

Brillouin function for comparison. Since all molecules have their trigonal axes parallel to the crystal c-axis, the experimentally determined magnetization along the c-axis is identical to that of the single molecule. The $M(H)$ measurements have been scaled to the saturation magnetization M(10 kOe) = 5 μ_B/fu.

The experimental $M(H)$ data at these three temperatures can be fitted well using a spin Hamiltonian for an S = 5/2

molecular ground state in a C_3 symmetry crystal-field, including zero-field splitting and a Zeeman interaction term:

$$H_{cl} = DS_z^2 - B_4^3O_4^3 - g\mu_B S_z H_z \quad (1)$$

yielding a crystal field cluster anisotropy $D/k_B = -0.47$ K $\pm$ 0.05 K (-0.33 cm^{-1}) and $g = 2.00$. The higher order term $B_4^3O_4^3$ provides a negligible contribution to the magnetization at these temperatures, however for the dynamics at $T < 1$ K it will be shown to be significant, *vide infra*. The $M(H)$ curves measured with a conventional SQUID on a powder sample of **1a** over the 1.8−8 K temperature range could also be simulated well using the same parameters (Figure S2).

These parameters are in good agreement with those obtained from the HF-EPR study:[51] $g = 2.00(1)$ and $D = -0.36$ cm^{-1}. Our parameters are also comparable to those recently reported by Hale et al.[32] from the fitting of $M(H)$ data measured on a powder sample in the 1.8−10 K range with $g = 1.98$, $D = -0.42$ cm^{-1}.

On the other hand, the susceptibility-temperature product $\chi T(T)$ measured between 1.8 and 300 K for a powdered sample of **1a** could be well explained under the coupling model shown in Figure S1, incorporating four antiferromagnetic (AF) exchange parameters J_1−J_4, with the exchange constants calculated by Hale et al.[32] (see Figure S3a).

Our crystallographic determination of the structure was performed at $T = 100$ K; i.e., below 173 K at which the measurements by Hale et al.[32] were performed (CCDC 2164410). The results are similar (see Table S1). A Peierls transition implies abrupt pairing of spins at finite temperatures that gives rise to abrupt jumps in the magnetic susceptibility.[59,60] Such an abrupt jump has not been observed in our magnetic measurements above or below 100 K or at even lower temperatures, as shown in Figure S3 of the Supporting Information. So, we can disregard this type of transition.

The emerging model is that of a Fe^{III}_7 cluster with peripheral Fe moments AF coupled, thus providing a zero contribution to the net magnetic moment. From our analysis, it is concluded that the cartwheel $S = 5/2$ magnetic ground state is then split by the crystal field into three Kramers' doublets with $|5/2, \pm 5/2\rangle$ as the lowest doublet and $|5/2, \pm 3/2\rangle$ as the first excited doublet located at $\Delta E = 4|D|/k_B \approx 2$ K.

Since we deal with Fe(III) ions with a high spin $S = 5/2$, the Fe orbital moment is in general negligible. However, as in the present case, anisotropy constants of the order of tenths of K ($|D|/k_B \cong 0.30$−0.6 K) are found in $Fe(III)_n$ clusters.[61] This magnetic anisotropy probably arises from the single-ion anisotropies of the 7 coupled Fe ions and from intramolecular dipolar interactions. The second-order Dzyaloshinskii−Moriya interaction (DMI) is much smaller than the Fe−Fe exchange interactions involved, which range between 5 and 40 cm^{-1}. Besides it is a current discussion about whether Fe^{III} compounds show DMI or only dipolar interactions.[62]

AC Magnetic Susceptibility. The in-phase component of the ac susceptibility as a function of temperature down to 0.1 K at different frequencies, $\chi'(T, f)$, measured under zero applied field for a powder sample of **1a** is shown in Figure 3a. The data show superparamagnetic behavior down to a blocking temperature T_B that depends on the frequency f of the ac field; T_B increases with increasing frequency, as expected for spins relaxing via a phonon-assisted process.

The out-of-phase components, $\chi''(T, f)$ (Figure 3b), also have frequency-dependent maxima, each at T_B^{max} ($\omega = 2\pi f$),

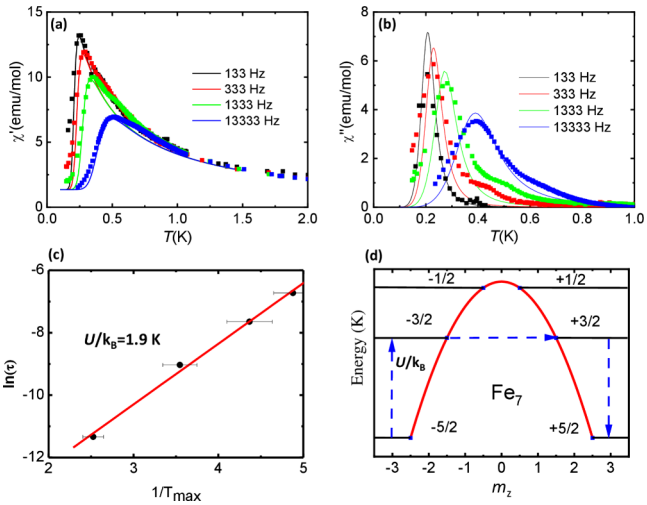

Figure 3. (a) In-phase and (b) out-of-phase components of the ac susceptibility of **1a**, measured as a function of temperature under $H = 0$, at different frequencies. The solid lines show the ac susceptibility calculated, using the model described in the text, for randomly oriented molecules relaxing via thermally activated quantum tunneling (TAQT). (c) Logarithm of the relaxation time as a function of the inverse temperature fitted to an Arrhenius law giving an activation energy barrier $U/k_B = 1.9$ K. (d) Schematics of the relaxation process in **1a** through a TAQT process.

and a small shoulder at about $T = 0.4$ K, which also shifts in temperature as a function of frequency. The shoulder could be due to a small fraction of the clusters having slightly different relaxation rates, as was reported for some Mn_{12} SMMs.[63] We assign the blocking temperature $T_B = 0.21$ K to the maximum of the $\chi''(T, f)$ curve at $f = 133$ Hz. This behavior is characteristic of a spin system with a well-defined spin relaxation time τ. Then, the ac susceptibility can be described by the well-known Debye law:

$$\chi = \chi_S + \frac{\chi_T - \chi_S}{1 + i\omega\tau} \quad (2)$$

where χ_S and χ_T are respectively the high-frequency and equilibrium limits of the susceptibility. The χ'' maxima can be used to get an estimate of τ, since $\tau\omega = 1$ approximately holds at $T = T_B^{max}$. The results are shown in Figure 3c. The spin relaxation time follows an Arrhenius law:

$$-\ln \omega = \ln \tau = \ln \tau_0 + U/k_B T_{max} \quad (3)$$

that is characteristic of relaxation taking place via a thermally activated process. Fitting the data using eq 3 gives the activation energy $U/k_B = 1.9 \pm 0.1$ K and the prefactor $\tau_0 = 10^{-7}$ s. Comparing U with the level scheme derived from the spin Hamiltonian (see Figure 3d), suggests that relaxation involves spin tunneling via the $m_z = \pm 3/2$ excited state.

In order to understand these results, it is of crucial importance to consider the proper C_3 symmetry of the spin Hamiltonian (1). Previous studies of this molecule have only considered it as purely uniaxial[27] or orthorhombic, with second-order off-diagonal terms.[51] Within these approximations, tunneling between $m_z = \pm 3/2$ is largely forbidden. By contrast, the term $B_4^3O_4^3$ allowed by the C_3 symmetry, opens this tunneling path. Tunneling through the $m_z = \pm 5/2$ doublet is, in principle, forbidden even in this case. However, this selection rule can be partly lifted if one considers the effect of environmental magnetic fields. Even though the ac suscepti-

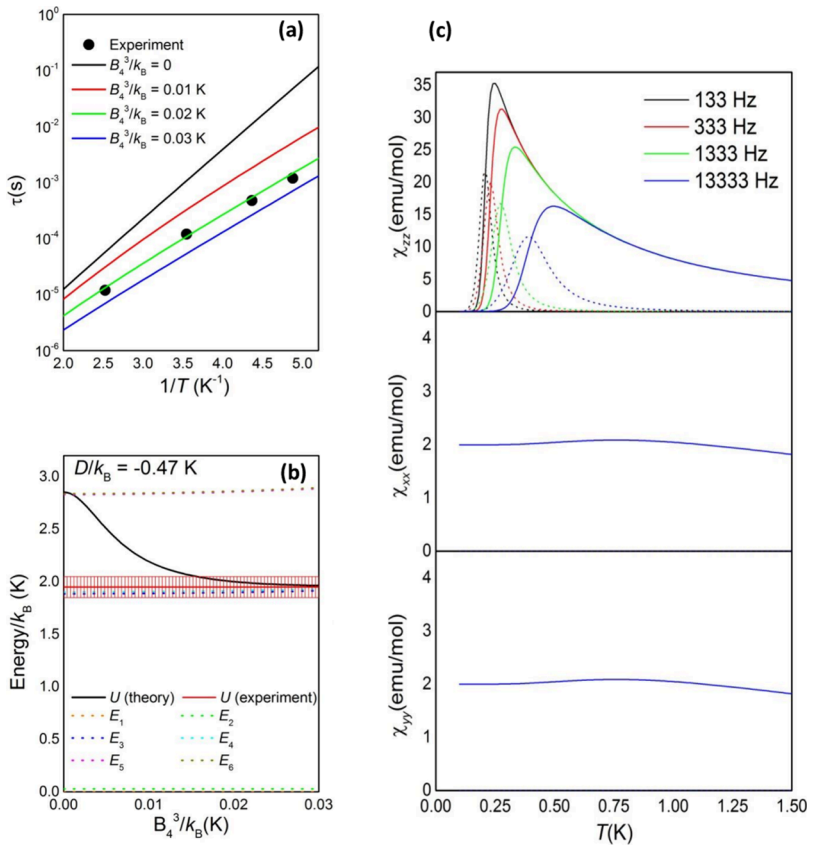

Figure 4. (a) Calculated relaxation time τ vs T^{-1} for different values of B_4^3/k_B (colored lines) in comparison with the experimental data for **1a** (black dots). (b) Activation energy calculated for **1a** as a function of the fourth-order off-diagonal anisotropy parameter B_4^3. The energies of the six magnetic states, $2S + 1 = 6$ for $S = 5/2$ (dotted lines), and the activation energy determined experimentally (red horizontal line, with the experimental error depicted as a colored band) are also shown. (c) Calculated ac susceptibilities in the three principal directions χ_{xx}, χ_{yy}, and χ_{zz} (χ' solid lines, χ'' dotted lines).

bility measurements were performed under zero applied field, dipole−dipole interactions with neighboring molecules generate additional terms. As a first approximation, these interactions can be taken into account by adding a dipolar effective field H_d to the Zeeman interaction in the spin Hamiltonian (1). Different components of H_d have a different influence on the spin tunneling probabilities. On the one hand, H_{dx} and H_{dy} enable tunneling between states, like $m_z = \pm 5/2$, for which $B_4^3O_4^3$ alone would not give any tunneling probability (see details in ref 64). On the other hand, H_{dz} suppresses tunneling via the ground state that would only occur at exactly $H_z = 0$. As typical values of the different components of H_d, we have taken $H_{dz} = g\mu_B S/c^3 \approx 42$ Oe, that is, equal to the field created by a nearest neighbor molecule located at a distance c = 10.40 Å, and $H_{d\perp} = g\mu_B S/\Lambda^3 \approx 12$ Oe, where Λ = 15.54 Å is the distance to a n.n.n. molecule. This approach is justifiable if the anisotropy axes of the molecular clusters point along the c-axis.[65] In any case, the results do not critically depend on the actual values taken for H_{dz} and $H_{d\perp}$.

We can put this idea on a more quantitative basis by means of a theoretical model[64,66,67] that incorporates thermally activated processes between exact eigenstates of the full spin Hamiltonian (1) into a quantum master equation. The numerical diagonalization of a Pauli's master equation that governs the time-dependent populations of the magnetic energy levels, provides the relaxation times τ_λ associated with the multiple (2S) spin relaxation modes (see Section S4 in S.I. for details). One of these modes characterizes the slow spin reversal process, with a time scale τ_1 close to that measured experimentally while all others are typically much faster. An important point is that the states used are exact energy eigenstates of the full Hamiltonian, which enables calculations to be performed under weak and strong magnetic fields or when tunneling probabilities are relatively high. As discussed in S4, the calculations show that the contributions to the susceptibility from fast relaxing modes[68] can be neglected in this case. Then, the complex ac susceptibility may be written as the Debye eq 2 with $\tau = \tau_1$ and $\chi_S = \chi_{VV}$ the van Vleck susceptibility. The latter arises from the effect of the magnetic field on the wave functions of the energy states.

The relaxation times calculated for different values of the fourth-order anisotropy parameter B_4^3 are shown in Figure 4a. The energies of the $2S + 1 = 6$ eigenstates of the spin Hamiltonian (eq 1) are given in Figure 4b as a function of B_4^3. For $B_4^3 = 0$, we obtain $E_{3/2}$ = 1.9 K, and $E_{1/2}$ = 2.84 K. The relaxation times approximately follow the Arrhenius law (3) with an activation energy U that decreases as B_4^3 increases, as it is also shown in Figure 4b. As we have mentioned above, increasing B_4^3 promotes tunneling via the $m_z = \pm 3/2$ states with respect to the classical thermally activated relaxation over the full barrier (i.e., via $m_z = \pm 1/2$ states). In order to match the experimental U/k_B = 1.9(1) K, values of $B_4^3/k_B \geq 0.015$ K are required, thus pointing to the presence of strong tunneling terms in this cluster.

Thus, the model ends up with just one dominant, slow relaxation time $\tau = \tau_o \exp(-U/k_BT)$. With these parameters,

the in-phase χ' and out-of-phase χ'' magnetic susceptibility components were calculated, for any orientation of the ac field, by solving the quantum master equation and then applying Debye eq 2. Figure 4c shows results obtained for the three principal directions χ_{xx}, χ_{yy}, and χ_{zz}. As it is well-known, only the longitudinal susceptibility (i.e., measured along the anisotropy axis) depends on frequency whereas the transverse susceptibility mainly contributes to χ_S. Since the experiments were performed on a powdered sample, we have to average over the random distribution of anisotropy axes. For the linear response, the averaged susceptibility gives

$$\chi = \frac{1}{3}\chi_{zz} + \frac{2}{3}\left(\frac{1}{2}\chi_{xx} + \frac{1}{2}\chi_{yy}\right) \quad (4)$$

The χ' and χ'' magnetic susceptibility contributions were calculated by solving the quantum master equation and then applying Debye eq 2 (see Section S4). As Figure 3a,b shows, the experimental data can be excellently reproduced for an anisotropy value $D/k_B \approx -0.47 \pm 0.02$ K, and $\chi_{VV} = 2.0$ emu/mol Oe in very good agreement to that estimated from the fit of the equilibrium magnetization data at low T ($D/k_B = -0.47 \pm 0.05$ K) (vide supra).

As regards the observation of magnetic hysteresis in a SMM, we note that at the lowest temperature where we have measured $M(H)$; i.e., $T = 0.38$ K, this system remains in the paramagnetic regime. Therefore, one does not expect to observe magnetic hysteresis at that temperature if the blocking temperature is as low as $T_B = 0.21$ K. On the other hand, the observation of nonzero χ'' below T_B is indeed a signal of SMM behavior since χ'' is proportional to the area of the magnetization loop induced by the oscillatory field. Thus, we can conclude that the Fe^{III}_7 cartwheel cluster **1a** behaves as a SMM, with a slow relaxation process due to thermally activated assisted tunneling (TAQT). We note that the SMM behavior in (**1a**) could not be detected by Hale et al.[32] since ac susceptibility measurements performed by these authors were limited to 1.8 K, of the same order than the activation energy.

Mössbauer Spectroscopy. The Mössbauer spectra of a polycrystalline sample of **1a** measured between 375 and 77 K under zero applied field are shown in Figure 5a. The electron relaxation covered almost the whole temperature range up to 375 K, as can be seen from the line-width values. The spectra down to 150 K are typical for three overlapped doublets each with a distinct isomer shift (δ_{Fe}) and quadrupole splitting (ΔE_Q), as a result of motional narrowing of the lines in fast relaxation condition with respect to the Larmor precession time $\tau_L \sim 10^{-8}$ s. The spectra were fitted to three doublets with relative intensity 1:3:3 as derived from the occupancy of the three different types of Fe^{III} sites (Figure 5b). The obtained δ_{Fe} and ΔE_Q are given in Table 1. The δ_{Fe} values are typical for $S = 5/2$ Fe^{III} ions and decrease with increasing temperature,[69] see also Table 1. Thus, the existence of three different types of Fe^{III}, as suggested by the crystal structure determination, is also confirmed by MS. The spectrum at 77 K shows a full spin−lattice relaxation process and therefore was not fitted.

In Figure 5b, the low temperature spectra (10 and 3 K) under $H = 0$ exhibit three sextets, for which the line-widths evidence the system is still relaxing. Narrower lines and better separation appear under increasing applied field. The Mössbauer parameters δ_{Fe} and ΔE_Q obtained for the three sextets at $T = 3$ K are summarized in Table 1. Since the coordination is octahedral for all Fe^{III} ions, the different relaxation time found for each sextet is mainly influenced by

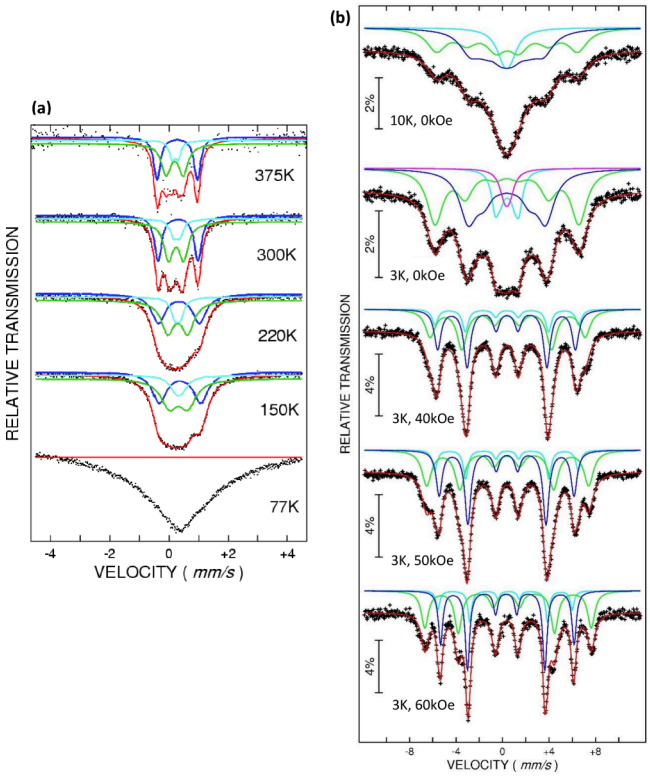

Figure 5. ^{57}Fe Mössbauer spectra for **1a**. (a) In zero-field at indicated temperatures. (b) At $T = 10$ K and $T = 3$ K in zero-field and for the latter temperature under magnetic fields of 40, 50, and 60 kOe.

the type of Fe neighbors and the Fe-ligand bond strength. The splitting of the three sets of sextet lines are discernible in the velocity ranges of roughly ±8, ±4 and, respectively, ±2 mm·s^{-1}, as shown in Figure 5b, at 3 K and $H = 0$. It can be seen from the lineshapes that the relaxation covers the whole investigated temperature range, including both the intracluster magnetic incipient ordering (10 and 3 K, Figure 5b) as well as the paramagnetic region (77−375 K), with highest effect at 77 K (Figure 5a).

The correct assignment of the Mössbauer doublets/sextets to the three distinct types of octahedrally coordinated Fe^{III} centers (Figure 6b) is clearly crucial for the determination of the spin structure. Doublet 1 can be readily assigned to the central Fe(1) since the ratios of the different Fe environments is 1:3:3. The other two doublets, 2 and 3, can be assigned through consideration of their respective quadrupole splittings (ΔE_Q) and isomer shifts (δ_{Fe}) using the values in Table 1 for $T = 150-300$ K. These parameters have been shown to correlate with values from bond length distortion (BLD) and bond valence sum (BVS) analyses, respectively, for a given Fe^{III} center.[70−73] These are listed and compared to the Mössbauer parameters in Table 2. The ΔE_Q parameter is also sensitive to the variation in strength of the six Fe−O/N bonds.[74]

For the central Fe(1) the six Fe−O bond lengths are similar, which results in the smallest BLD. Fe(3) also has O_6 coordination with the bond lengths giving a larger BLD, while Fe(2), with its O_5N coordination, has the largest BLD of the three Fe^{III} types. In the spectra of **1a**, the ΔE_Q parameters are quite different for the three Fe sites in the molecule, and from the values given in Table 2, it is clear that the quadrupole splitting ΔE_Q follows the same trend as the BLD values. In addition the X−Fe−X angles around Fe(2), 78.3(4)−98.3(4)°

Table 1. Parameters of the Mössbauer Spectra as a Function of Applied Field (H_{appl}) and Temperature for 1a[d]

H_{appl} (kOe)	T (K)	pattern	$\lvert H_{eff}\rvert$ (kOe)	H_{int} (kOe)	δ_{Fe}[a] (mm/s)	ΔE_Q (mm/s)	Γ (mm/s)	θ (deg)	area (%)
0.0	300	doublet 1	0		0.369(5)	0.21(1)	0.29(2)		14.28
		doublet 2	0		0.415(1)	1.345(3)	0.29(3)		42.85
		doublet 3	0		0.350(2)	0.508(9)	0.377(7)		42.85
0.0	220	doublet 1	0		0.403(3)	0.191(8)	0.29(1)		14.28
		doublet 2	0		0.448(2)	1.373(7)	0.547(9)		42.85
		doublet 3	0		0.401(2)	0.663(9)	0.52(1)		42.85
0.0	150	doublet 1	0		0.446(4)	0.21(2)	0.49(6)		14.28
		doublet 2	0		0.486(2)	1.403(7)	0.590(7)		42.85
		doublet 3	0		0.432(3)	0.63(2)	0.67(1)		42.85
0.0	3	sextet 1	53		0.48[b]	0.02(3)	1.13(5)	41.3[c]	14.28
		sextet 2	210		0.51[b]	0.02(1)	1.67(3)	41.3[c]	42.85
		sextet 3	393		0.47[b]	0.02(1)	1.69(3)	41.3[c]	42.85
40	3	sextet 1	383	−343	0.48[b]	−0.01(1)	0.59(3)	65.8[c]	14.28
		sextet 2	367	−327	0.51[b]	−0.042(8)	0.70(1)	65.8[c]	42.85
		sextet 3	413	+373	0.47[b]	0.08(1)	1.02(2)	65.8[c]	42.85
50	3	sextet 1	383	−233	0.48[b]	−0.064(9)	0.49(1)	71.6	14.28
		sextet 2	360	−310	0.51[b]	−0.028(4)	0.626(7)	80.7	42.85
		sextet 3	432	+382	0.47[b]	0.083(8)	0.98(1)	62.2	42.85
60	3	sextet 1	358	−298	0.48[b]	−0.30(1)	0.39(1)	81.0	14.28
		sextet 2	356	−296	0.51[b]	0.101(7)	0.450(1)	73.9	42.85
		sextet 3	443	+383	0.47[b]	0.14(1)	0.74(1)	63.0	42.85

[a]Relative to α-Fe at room temperature. The statistical errors are given in parentheses. The relative areas for the spectra have been constrained to the 1:3:3 ratio. [b]Fixed (constrained) values. [c]Fixed to be equal for all Fe sites. Γ: line width at half-maximum. In column 3, doublets (sextets) 1, 2, and 3 correspond to Fe(1), Fe(2), and Fe(3), respectively. [d]The spectra measured at 10 and 3 K at H = 0 were not considered for the parameter optimization because of apparent relaxation broadening.

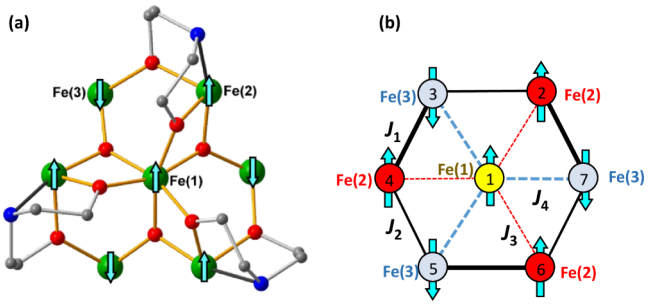

Figure 6. (a) Spin structure for **1a** obtained from the Mössbauer study, which confirms that proposed by Hale et al.[32] for the coupling scheme shown in (b). The four interactions constants (J_1–J_4) were found to be antiferromagnetic, with $|J_1| > |J_4| > |J_2| > |J_3|$ (see details in S2).

Table 2. Bond Length Distortions (BLD) and Bond Valence Sum (BVS) Calculation Parameters for the Fe(1), Fe(2), and Fe(3) Sites in 1a in Combination with Mössbauer Parameters at 300 K

Fe site	BLD	ΔE_Q (mm/s) 300 K	BVS	δ_{Fe} (mm/s) 300 K
Fe(1)	0.600	0.21(1)	3.19	0.369(5)
Fe(2)	3.672	1.345(3)	3.18	0.415(1)
Fe(3)	2.930	0.508(9)	3.22	0.350(2)

and 160.5(4)−174.5(4)° deviate more from 90 and 180 than those for Fe(3), 83.3(4)−96.3(4)° and 168.2(4)−174.9(4)°, which will also lead to a higher ΔE_Q. Furthermore, the presence of one covalent Fe−N bond in the coordination sphere of Fe(2) will also tend to increase ΔE_Q. On the basis of the ΔE_Q values doublet 2 can therefore be assigned to Fe(2) and doublet 3 to Fe(3).

The isomer shift (δ_{Fe}) is mostly governed the electron density near the nucleus (s-electrons), which perturb the nuclear charge. The bond valence sum (BVS) for an Fe^{III} should therefore show an inverse correlation with δ_{Fe}, since a larger electron density near the nucleus will increase δ_{Fe}.[74] From Table 2 the variation in the BVS values is rather low, but the Fe(2) does have the lowest BVS value and doublet 2 the highest δ_{Fe}'s, probably reflecting the different O_5−N coordination, which is consistent with the assignments previously made from the ΔE_Q values.

For Fe^{III}, the internal field, $\vec{H}_{int}$, results from the Fermi contact interaction between the nucleus and the s-electron density, and dominates over other terms. It encompasses the effect due to its own magnetic moment and that of the neighboring atoms, and is negative; i.e., it is opposed to the magnetic moment of the ion. When an external magnetic field $\vec{H}_{appl}$ is applied, the observed hyperfine field $\vec{H}_{eff}$ is the vector sum of the internal and applied fields:

$$\vec{H}_{eff} = \vec{H}_{int} + \vec{H}_{appl} \quad (5)$$

Thus, the variation of the Mössbauer spectra measured as a function of an increasing magnetic field allows the determination of the relative orientations of the Fe^{III} spins within the cluster. For clarity, the individual sextets in Figure 5b are drawn with the same colors as the corresponding doublets in Figure 5a from which they result on application of a magnetic field.

On inspection of data measured at T = 3 K under different H_{appl} (Figure 5b and Table 1) it is observed that, with increasing magnetic applied field, two of the three sextets (corresponding to doublets 1 and 2) show an inward evolution of the positions of the lines, thus demonstrating antiparallel orientation to the field, showing that the internal field from the

unpaired d-electrons is oriented antiparallel to the applied field.[75]

However, the third sextet (corresponding to doublet 3) shows the reverse behavior, with an outward displacement of sextet lines on increasing applied field, with the spins of the d-electrons now parallel to the applied field. Thus, given our previous assignment of the doublets, it is clear that the spins on Fe(1) and the three Fe(2) are all oriented coparallel, with those on the three Fe(3) antiparallel to those of Fe(1) and Fe(2) (Figure 6). The Mössbauer study presented here thus provides direct experimental confirmation of the spin structure proposed by Hale et al.,[32] leading to the observed total spin S = 5/2 for the Fe_7 cluster.

At 3 K, when the magnetic field is applied perpendicular to the γ-radiation direction and parallel to sample plane, the increased intensities of the $\Delta m = 0$ lines (lines 2 and 5 of the sextet) increase relative to the others, suggesting that the magnetic moments are orienting toward the applied field, as expected. In the case when the quadrupole interaction represents a small perturbation and the absorber thickness is negligible, then for ^{57}Fe the relative intensities of the outer, middle and inner pairs of lines making up the sextet lines (R1, lines 1 and 6; R2, lines 2 and 5; R3, lines 3 and 4) are given by

$$R1 = 3(1 + \cos^2\theta) \tag{6a}$$

$$R2 = 4\sin^2\theta \tag{6b}$$

$$R3 = (1 + \cos^2\theta) \tag{6c}$$

For a given sextet, made up of lines 1−6, where 1 and 6 are the outer lines, the ratio of the intensities of lines 2 and 5 of the sextet (R2) compared to those of the two central lines 3 and 4 (R3) yields information on the angle θ between H_{eff} and the incident γ rays, and hence the direction of the magnetic moments versus γ-rays.[76,69] This ratio R2/R3 can take values from zero (when the magnetic moment is parallel to the incident γ-radiation and perpendicular to the sample plane) up to four (when the magnetic moment lies within the plane of the sample). It should be noted that for measurements performed on polycrystalline samples or powders that have been carefully grounded to make a homogeneous Mössbauer absorber, the intensity ratios within each sextet show smaller values than the theoretical ones (3:2:1)[77] for a random distribution calculated from Clebsch−Gordan coefficients. The calculated θ values for each sextet are collected in Table 1. One notes that the angle increases practically to a parallel alignment with the applied field for sextets 1 and 2, that is for atom sites Fe(1) and Fe(2), while it is noticeably smaller for sextet 3, i.e., for Fe(3). This result further supports the result of the analysis of the H_{eff} dependence on increasing field given above; i.e., Fe(1) and Fe(2) have their respective spins parallel to each other, while those on Fe(3) are antiparallel.

The intracluster interactions were previously proposed to be AF in the trend $|J_1| > |J_4| > |J_2| > |J_3|$, where J_1 and J_4 are comparable in intensity, J_2 is intermediate and J_3 is weak.[32] This scheme is represented in Figure 6b, by the intensities of the lines depicting the exchange paths. The cartwheel spin configuration may be envisaged as comprising six triangles, each sharing two of their sides. When the intra-atomic couplings are AF one may expect the appearance of frustration. This has been addressed in refs 40 and 27, which discuss the frustrated and unfrustrated cases giving rise to the different ground states possible, ranging from S = 1/2 to 35/2. In the present case, the AF J_1 and J_4 favor an unfrustrated coupling to a S = 5/2 ground state. The intermediate AF J_2 just reinforces their coupling, and thus to the S = 5/2 unfrustrated ground state. The weak AF J_3 coupling perturbs the ground state and may bring about some frustration, but in fact does not modify the S = 5/2 ground state. This kind of spin structure leading to a nonzero ground, enabled by coexisting competing AF interactions corresponds to Type III of frustration, according to Winpenny's definition.

The very large temperature range (from 3 K to somewhere above 120 K) of a fast spin−lattice relaxation, well-illustrated by the 77 K MS collapsed spectrum, is an evidence for complex interactions between each type of Fe^{III} in this hepta-nuclear molecule. Such a crossover from fast to slow relaxation regime, as temperature is lowered, is not unusual for high-spin Fe^{III}, particularly for small molecules because their spin−orbit-lattice relaxation can be essentially slow via a vanishing orbital moment.

From eq 3 it may be calculated that at T = 3 K the spin relaxation time is $\tau_s = 2 \times 10^{-7}$ s, which is an order of magnitude larger than the Larmor precession time $\tau_L \sim 10^{-8}$ s. This indicates that at 3 K even at $H_{appl} = 0$ we are in a slow relaxation regime, which is consistent with a blocking temperature of $T_B \cong 0.21$ K found from the magnetic susceptibility data.

CONCLUSIONS

Magnetic investigations using SQUID magnetometry down to 1.8 K, micro-Hall magnetometry down to 0.3 K, and ac susceptibility measurements down to 0.1 K were conducted on the "cartwheel" coordination cluster $[Fe^{III}_7O_3(O_2C^tBu)_9(Me\text{-}dea)_3(H_2O)_3]$ (**1a**). From the magnetization $M(H)$ curves measured on a single crystal it is concluded that the molecule has an S = 5/2 ground state with a uniaxial crystal field anisotropy $D/k_B = -0.47$ K, consistent with previous EPR findings.

The ac susceptibility results reveal a superparamagnetic behavior down to a blocking temperature $T_B \approx 0.21$ K. The experimental χ', χ'' (f, T) data could be fitted with a model considering quantum tunneling relaxation through the thermally excited $m_z = \pm 3/2$ doublet. The Fe_7 molecule shows SMM behavior which is consistent with its uniaxiality and with an activation barrier of $U/k_B = 1.9$ K.

^{57}Fe Mössbauer spectra of **1a** at 3 K exhibit three sextets, which could be unambiguously assigned to the three distinct Fe sites in the cluster. The isomer shift and quadrupole splitting parameter determination confirmed all the Fe^{III} to be in the S = 5/2 state. Narrower lines and better separation were observed under an applied magnetic field up to 6 T. Analysis with NORMOS code of the evolution of the sextets on increasing field showed that the spin on the central Fe(1) is parallel to those on the peripheral Fe(2) sites with O_5N coordination from the chelation by the Me-dea ligands, while the spins on the Fe(3) centers, with O_6 coordination, are antiparallel to those on Fe(1) and Fe(2). This provides experimental confirmation of the spin structure previously deduced from coupling constants by Hale et al.[32] According to Winpenny's definition, it corresponds to a Type III frustration case.

Spectral line broadening even at H = 0 and T = 3 K indicate that the spins are still far from blocking at this temperature, consistent with the blocking temperature (≈0.21 K) found from the susceptibility data.

These magnetic and Mössbauer studies have thus provided the final two pieces of experimental evidence and completed the magnetic analysis of $[Fe^{III}_7O_3(O_2C^tBu)_9(Medea)_3(H_2O)_3]$ (**1a**). This and previous studies on **1a** and analogous isostructural compounds demonstrate how a "multipronged" approach, bringing together a range of complementary experimental and theoretical techniques, leads to a complete magnetic description of this frustrated Fe^{III}_7 cartwheel system. Magnetic measurements at sub-Kelvin temperatures were crucial to prove the SMM behavior of this molecule.

AUTHOR INFORMATION

Corresponding Authors

Juan Bartolomé − *Instituto de Nanociencia y Materiales de Aragón (INMA), CSIC, Universidad de Zaragoza, Zaragoza 50009, Spain; Royal Academy of Sciences of Zaragoza, Zaragoza 50009, Spain;* orcid.org/0000-0002-6517-1236; Email: barto@unizar.es

Annie K. Powell − *Institute of Inorganic Chemistry, Institute of Nanotechnology (INT), and Institute for Quantum Materials and Technologies (IQMT), Karlsruhe Institute of Technology (KIT), Karlsruhe 76131, Germany;* orcid.org/0000-0003-3944-7427; Email: annie.powell@kit.edu

Authors

Elena Bartolomé − *Institut de Ciència de Materials de Barcelona (ICMAB)-CSIC, Bellaterra, Barcelona 08193, Spain;* orcid.org/0000-0001-5108-0977

Fernando Luis − *Instituto de Nanociencia y Materiales de Aragón (INMA), CSIC, Universidad de Zaragoza, Zaragoza 50009, Spain; Royal Academy of Sciences of Zaragoza, Zaragoza 50009, Spain;* orcid.org/0000-0001-6284-0521

Enrique Burzurí − *Departamento de Física de la Materia Condensada and Condensed Matter Physics Center (IFIMAC), Universidad Autónoma de Madrid, Madrid 28049, Spain; Instituto Universitario de Ciencia de Materiales "Nicolás Cabrera" (INC), Universidad Autónoma de Madrid, Madrid E-28049, Spain;* orcid.org/0000-0001-7906-7192

Agustin Camón − *Instituto de Nanociencia y Materiales de Aragón (INMA), CSIC, Universidad de Zaragoza, Zaragoza 50009, Spain*

[¶]**George Filoti** − *National Institute of Materials Physics, Bucharest, Magurele 077125, Romania*

Ayuk M. Ako − *Institute of Inorganic Chemistry, Karlsruhe Institute of Technology (KIT), Karlsruhe 76131, Germany*

Jonas Braun − *Institute of Inorganic Chemistry, Institute of Nanotechnology (INT), and Institute for Quantum Materials and Technologies (IQMT), Karlsruhe Institute of Technology (KIT), Karlsruhe 76131, Germany*

Valeriu Mereacre − *Institute of Inorganic Chemistry, Karlsruhe Institute of Technology (KIT), Karlsruhe 76131, Germany;* orcid.org/0000-0002-8295-6078

Christopher E. Anson − *Institute of Inorganic Chemistry, Karlsruhe Institute of Technology (KIT), Karlsruhe 76131, Germany;* orcid.org/0000-0001-7992-7797

Author Contributions

Conceptualization of the study: J.B. and A.K.P. Synthesis: A.M.A. Crystallography: C.E.A. Magnetometry: J.B., F.L., E.Bu., A.C. Mössbauer spectroscopy: G.F., V.M. Analysis and manuscript preparation: J.B., E.Ba., J.B., C.E.A., A.K.P. The manuscript was written through contributions of all authors. All authors have given approval to the final version of the manuscript.

Notes

The authors declare no competing financial interest.

[¶]Prof. G. Filoti passed away on March 17, 2021.

ACKNOWLEDGMENTS

The authors acknowledge grants PID2022-138492NB-I00 and PID2022-140923NB-C21&C22 funded by MCIN/AEI/10.13039/501100011033s, ERDF "A way of making Europe" and ESF "Investing in your future", Gobierno de Aragón (grant E09-17R-Q-MAD and RASMIA project E12-23R), the Advanced Materials program funded by the European Union Next GenerationEU (PRTR-C17.I1), MCIN and Gobierno de Aragón, and the State Research Agency, through the Severo Ochoa Program for Centres of Excellence in R&D (CEX2023-001263-S and CEX2023-001286-S). A.M.A., J.B., V.M., C.E.A., and A.K.P. acknowledge funding from the Helmholtz Foundation POF MSE. This paper is dedicated to the memories of the late Prof. G. Filoti (1942−2021) NIMP, Bucharest-Magurele, Romania, and Prof. N. Turta (1940−2015), Institute of Chemistry, Academy of Sciences, Chisenau, Moldavia.

REFERENCES

(1) Gatteschi, D.; Sessoli, R.; Cornia, A. Single-Molecule Magnets Based on Iron(III) Oxo Clusters Dedicated to the Memory of Professor Olivier Kahn. *Chem. Commun.* **2000**, *9*, 725−732.

(2) Taft, K. L.; Lippard, S. J. Synthesis and Structure of [Fe(OMe)2(O2CCH2Cl)]10: A Molecular Ferric Wheel. *J. Am. Chem. Soc.* **1990**, *112*, 9629.

(3) Gatteschi, D.; Caneschi, A.; Sessoli, R.; Cornia, A. A. Magnetism of Large Iron-Oxo Clusters. *Chem. Soc. Rev.* **1996**, *25*, 101−109.

(4) Stamatatos, T. C.; Christou, A. G.; Mukherjee, S.; Poole, K. M.; Lampropoulos, C.; Abboud, K. A.; O'Brien, T. A.; Christou, G. High-Yield Syntheses and Reactivity Studies of Fe10 "Ferric Wheels":: Structural, Magnetic, and Computational Characterizaton of a Star-Shaped Fe8 Complex. *Inorg. Chem.* **2008**, *47*, 9021.

(5) Lee, K. H. K.; Aebersold, L.; Peralta, J. E.; Abboud, K. A.; Christou, G. Synthesis, Structure, and Magnetic Properties of an Fe36 Dimethylarsinate Cluster: The Largest "Ferric Wheel. *Inorg. Chem.* **2022**, *61*, 17256−17267.

(6) Caneschi, A.; Cornia, A.; Fabretti, A. C.; Gatteschi, D. Structure and Magnetic Properties of a Dodecanuclear Twisted-Ring Iron(III) Cluster. *Angew. Chem., Int. Ed.* **1999**, *39*, 1295−1297.

(7) Saalfrank, R. W.; Bernt, I.; Uller, E.; Hampel, F. Template-Mediated Self Assembly of Six- and Eight-Membered Iron Coronates. *Angew. Chem., Int. Ed. Engl.* **1997**, *36*, 2482.

(8) Sydora, O. L.; Woleczanski, P. T.; Lobkovsky, E. B. Ferrous Wheels, Ellipse [(TBu3SiS)FeX]n, and Cube [(TBu3SiS)Fe-(CCSitBu3)]4. *Angew. Chem., Int. Ed.* **2003**, *42*, 2685−2687. and references cited therein.
(9) Cañada-Vilalta, C.; O'Brien, T.; Brechin, E.; Pink, M.; Davidson, E.; Christou, G. Large Spin Differences in Structurally Related Fe6 Molecular Clusters and Their Magnetostructural Explanation. *Inorg. Chem.* **2004**, *43* (18), 5505−5521.
(10) Watton, S. P.; Fuhrmann, P.; Pence, L. E.; Caneschi, A.; Cornia, A.; Abbati, G. L.; Lippard, S. J. A Cyclic Octadecairon(III) Complex, the Molecular 18-Wheeler. *Angew. Chem., Int. Ed. Engl.* **1997**, *36*, 2774.
(11) Jones, L. F.; Low, D. M.; Helliwell, M.; Raftery, J.; Collison, D.; Aromí, G.; Cano, J.; Mallah, T.; Wernsdorfer, W.; Brechin, E. K.; et al. Fe(III) Clusters Built with Tripodal Alcohol Ligands. *Polyhedron* **2006**, *25* (2), 325−333.
(12) King, P.; Stamatatos, T. C.; Abboud, K. A.; Christou, G. Reversible Size Modification of Iron and Gallium Molecular Wheels: A Ga10 "Gallic Wheel" and Large Ga18 and Fe18 Wheels. *Angew. Chem., Int. Ed.* **2006**, *45*, 7379.
(13) Yao, H. C.; Wang, J. J.; Ma, Y. S.; Waldmann, O.; Du, W. X.; Song, Y.; Li, Y. Z.; Zheng, L. M.; Decurtins, S.; Xin, X. Q. An Iron(III) Phosphonate Cluster Containing a Nonanuclear Ring. *Chem. Commun.* **2006**, *16*, 1745−1747.
(14) Taft, K. L.; Delfs, C. D.; Papaefthymiou, G. C.; Foner, S.; Gatteschi, D.; Lippard, S. J. [Fe(OMe)2(O2CCH2Cl)]10, a Molecular Ferric Wheel. *J. Am. Chem. Soc.* **1994**, *114* (3), 823−832.
(15) Cornia, A.; Affronte, M.; Jansen, A. G. M.; Abbati, G. L.; Gatteschi, D. Tuning of Magnetic Anisotropy in Hexairon(III) Rings by Host-Guest Interactions: An Investigation by High-Field Torque Magnetometry. *Angew. Chem., Int. Ed.* **1999**, *38*, 2264.
(16) Waldmann, O.; Schülein, J.; Koch, R.; Müller, P.; Bernt, I.; Saalfrank, R. W.; Andres, H. P.; Güdel, H. U.; Allenspach, P. Magnetic Anisotropy of Two Cyclic Hexanuclear Fe(III) Clusters Entrapping Alkaline Ions. *Inorg. Chem.* **1999**, *38*, 5879.
(17) Waldmann, O.; Koch, R.; Schromm, S.; Schülein, J.; Müller, P.; Bernt, I.; Saalfrank, R. W.; Hampel, F.; Balthes, E. Magnetic Anisotropy of a Cyclic Octanuclear Fe(III) Cluster and Magneto-Structural Correlations in Molecular Ferric Wheels. *Inorg. Chem.* **2001**, *40*, 2986.
(18) Waldmann, O. Spin Dynamics of Finite Antiferromagnetic Heisenberg Spin Rings. *Phys. Rev. B* **2002**, *65*, No. 024424.
(19) Waldmann, O.; Guidi, T.; Carretta, S.; Mondelli, C.; Dearden, A. Elementary Excitations in the Cyclic Molecular Nanomagnet Cr8. *Phys. Rev. Lett.* **2003**, *91*, No. 237202.
(20) Waldmann, O. Magnetic Molecular Wheels and Grids - the Need for Novel Concepts in "Zero-Dimensional" Magnetism. *Coord. Chem. Rev.* **2005**, *249*, 2550.
(21) Waldmann, O.; Dobe, C.; Mutka, H.; Furrer, A.; Güdel, H. U. Neel-Vector Tunneling in Antiferromagnetic Molecular Clusters. *Phys. Rev. Lett.* **2005**, *95*, No. 057202.
(22) Troiani, F.; Affronte, M.; Carretta, S.; Santini, P.; Amoretti, G. Proposal for Quantum Gates in Permanently Coupled Antiferromagnetic Spin Rings without Need of Local Fields. *Phys. Rev. Lett.* **2005**, *94*, No. 190501.
(23) Troiani, F.; Ghirri, A.; Affronte, M.; Carretta, S.; Santini, P.; Amoretti, G.; Piligkos, S.; Timco, G.; Winpenny, R. E. P. Molecular Engineering of Antiferromagnetic Rings for Quantum Computation. *Phys. Rev. Lett.* **2005**, *94* (20), No. 207208.
(24) Oshio, H.; Hoshino, N.; Ito, T.; Nakano, M.; Renz, F.; Gütlich, P. High-Spin Wheel of a Heptanuclear Mixed-Valent FeII,III Complex. *Angew. Chem., Int. Ed.* **2003**, *42*, 223.
(25) Saalfrank, R. W.; Deutscher, C.; Sperner, S.; Nakajima, T.; Ako, A. M.; Uller, E.; Hampel, F.; Heinemann, F. W. Six-Membered Metalla-Coronands. Synthesis and Crystal Packing: Columns, Compartments, and 3D-Networks. *Inorg. Chem.* **2004**, *43*, 4372.
(26) Jones, L. F.; Jensen, P.; Moubaraki, B.; Berry, K. J.; Boas, J. F.; Pilbrow, J. R.; Murray, K. S. J. Heptanuclear Iron(Iii) Triethanolamine Clusters Exhibiting 'Millennium Dome'-like Topologies and an Octanuclear Analogue with Ground Spin States of S = 5/2 and 0. *Respectively. J. Mater. Chem.* **2006**, *16*, 2690.
(27) Ako, A. M.; Waldmann, O.; Mereacre, V.; Klöwer, F.; Hewitt, I. J.; Anson, C. E.; Güdel, H. U.; Powell, A. K. Odd-Numbered FeIII Complexes: Synthesis, Molecular Structure, Reactivity, and Magnetic Properties. *Inorg. Chem.* **2007**, *46*, 756.
(28) Hoshino, N.; Ako, A.; Powell, A.; Oshio, H. Molecular Magnets Containing Wheel Motifs. *Inorg.Chem.* **2009**, *48*, 3396−3407.
(29) Mukherjee, S.; Bagai, R.; Abboud, K. A.; Christou, G. Raising the Spin of FeIII7 Disklike Clusters: The Power of Molecular Spin Frustration. *Inorg. Chem.* **2011**, *50*, 3849−3851.
(30) Kizas, C. M.; Papatriantafyllopoulou, C.; Pissas, M.; Sanakis, Y.; Javed, A.; Tasiopoulus, A.; Lampropoulos, C. Synthesis, Magnetic and Spectroscopic Characterization of a New Fe7 Cluster with a Six-Pointed Star Topology. *Polyhedron* **2013**, *64*, 280−288.
(31) Mondal, K.; Mereacre, V.; Kostakis, G.; Lan, Y.; Anson, C.; Prisecaru, I.; Waldmann, O.; Powell, A. K. A Strongly Spin-Frustrated FeIII7 Complex with a Canted Intermediate Spin Ground State of S = 7/2 or 9/2. *Chem.—Eur. J.* **2015**, *21*, 10835−10842.
(32) Hale, A. R.; Aebersold, L. E.; Peralta, J. E.; Foguet-Albiol, D.; Abboud, K. A.; Christou, G. Analysis of Spin Frustration in an FeIII7 Cluster Using a Combination of Computational, Experimental, and Magnetostructural Correlation Methods. *Polyhedron* **2022**, *225*, No. 116045.
(33) Hale, A.; Lott, M.; Peralta, J.; Foguet-Albiol, D.; Abboud, K.; Christou, G. Magnetic Properties of High-Nuclearity Fex-Oxo (X = 7, 22, 24) Clusters Analyzed by a Multipronged Experimental, Computational, and Magnetostructural Correlation Approach. *Inorg. Chem.* **2022**, *61* (29), 11261−11276.
(34) Schnack, J. Effects of Frustration on Magnetic Molecules: A Survey from Olivier Kahn until Today. *Dalton Trans.* **2010**, *39*, 4693−4707.
(35) Kahn, O. Competing Spin Interactions and Degenerate Frustration for Discrete Molecular Species. *Chem. Phys. Lett.* **1997**, *265*, 109−114.
(36) McCusker, J. K.; Vincent, J. B.; Schmitt, E. A.; Mino, M. L.; Shin, K.; Coggin, D. K.; Hagen, P. M.; Huffman, J. C.; Christou, G.; Hendrickson, D. N. Molecular Spin Frustration in the [Fe4O2]8+ Core: Synthesis, Structure, and Magnetochemistry of [Fe4O2-(O2CR)7(Bpy)2](ClO4) (R = Me, Ph). *J. Am. Chem. Soc.* **1991**, *113*, 3012−3021.
(37) Singh, A.; Joshi, R.; Abboud, K.; Peralta, J.; Christou, G. Molecular Spin Frustration in Mixed-Chelate Fes5 and Fe6 Oxo Clusters with High Ground State Spin Values. *Polyhedron* **2004**, *176*, No. 114182.
(38) Baker, M. L.; Timco, G. A.; Piligkos, S.; Mathieson, J. S.; Mutka, H.; Tuna, F.; Kozlowski, P.; Antkowiak, M.; Guidi, T.; Gupta, T.; et al. A Classification of Spin Frustration in Molecular Magnets from a Physical Study of Large Odd-Numbered-Metal, Odd Electron Rings. *Proc. Natl. Acad. Sci. U. S. A.* **2012**, *109*, 19113−19118.
(39) Cannon, R. D.; White, R. P. Chemical and Physical Properties of Triangular Bridged Metal Complexes. In *Progress in Inorganic Chemistry*; Lippard, S. J., Ed.; John Wiley & Sons, 1988; vol *36*, pp 195−298.
(40) Richter, J.; Voigt, A. J. The Spin- 1/2 Heisenberg Star with Frustration: Numerical versus Exact Results. *J. Phys. A Math. Gen.* **1994**, *27*, 1139.
(41) Richter, J.; Voigt, A.; Krüger, S. E.; Gros, C. The Spin- 1/2 Heisenberg Star with Frustration: II. The Influence of the Embedding Medium. *J. Phys. A Math. Gen.* **1996**, *29*, 825−836.
(42) Powell, A. K.; Heath, S. L.; Gatteschi, D.; Pardi, L.; Sessoli, R.; Spina, G.; Del Giallo, F.; Pieralli, F. Synthesis, Structures, and Magnetic Properties of Fe2, Fe17, and Fe19 Oxo-Bridged Iron Clusters: The Stabilization of High Ground State Spins by Cluster Aggregates. *J. Am. Chem. Soc.* **1995**, *117*, 2491−2502.
(43) Goodwin, J.; Sessoli, R.; Gatteschi, D.; Wernsdorfer, W.; Powell, A.; Heath, S.; Barra, A. Towards Nanostructured Arrays of Single Molecule Magnets:: New Fe19 Oxyhydroxide Clusters

Displaying High Ground State Spins and Hysteresis. *J. Chem. Soc., Dalton Trans.* **2000**, *24*, 1835−1840.
(44) Murugesu, M.; Clérac, R.; Wernsdorfer, W.; Anson, C. E.; Powell, A. K. Hierarchical Assembly of {Fe13} Oxygen-Bridged Clusters into a Close-Packed Superstructure. *Angew. Chem., Int. Ed.* **2005**, *44*, 6678−6682.
(45) Ako, A. M.; Mereacre, V.; Lan, Y.; Wernsdorfer, W.; Clerac, R.; Anson, C. E.; Powell, A. K. An Undecanuclear FeIII Single-Molecule Magnet. *Inorg. Chem.* **2010**, *49*, 1−3.
(46) Weighardt, K.; Pohl, K.; Jibril, I.; Huttner, G. Hydrolysis Products of the Monomeric Amine Complex (C6H15N3)FeCl3: The Structure of the Octameric Iron(III) Cation of {[(C6H15N3)6Fe8(M3-O)2(M2-OH)12]Br7(H2O)}Br·8H2O. *Angew. Chem. Int. Ed* **1984**, *23* (1), 77−78.
(47) Barra, A.; Debrunner, P.; Gatteschi, D.; Schulz, C.; Sessoli, R. Superparamagnetic-like Behavior in an Octanuclear Iron Cluster. *Europhys. Lett.* **1996**, *35*, 133−138.
(48) Barra, A.; Caneschi, A.; Cornia, A.; de Biani, F.; Gatteschi, D.; Sangregorio, C.; Sessoli, R.; Sorace, L. Single-Molecule Magnet Behavior of a Tetranuclear Iron(III) Complex. The Origin of Slow Magnetic Relaxation in Iron(III) Clusters. *J. Am. Chem. Soc.* **1999**, *121*, 5302−5310.
(49) Ruiz, E.; Rodríguez-Fortea, A.; Cano, J.; Alvarez, S. Theoretical Study of Exchange Coupling Constants in an Fe19 Complex. *J. Phys. Chem. Solids* **2004**, *65*, 799−803.
(50) Castelli, L.; Fittipaldi, M.; Powell, A. K.; Gatteschi, D.; Sorace, L. Single Crystal EPR Study at 95 GHz of a Large Fe Based Molecular Nanomagnet: Toward the Structuring of Magnetic Nanoparticle Properties. *Dalton Trans.* **2011**, *40*, 8145−8155.
(51) Datta, S.; Betancur-Rodriguez, A.; Lee, S.; Hill, S.; Foguet-Albiol, D.; Bagai, R.; Christou, G. EPR Characterization of Half-Integer-Spin Iron Molecule-Based Magnets. *Polyhedron* **2007**, *26*, 2243−2246.
(52) Mitchell, K. J.; Abboud, K. A.; Christou, G. Magnetostructural Correlation for High-Nuclearity Iron(III)/Oxo Complexes and Application to Fe5, Fe6, and Fe8 Clusters. *Inorg. Chem.* **2016**, *55*, 6597−6608.
(53) Sheldrick, G. M. *SADABS (the Siemens Area Detector Absorption Correction)*; University of Göttingen: Göttingen, Germany, 1996.
(54) Sheldrick, G. M. A Short History of SHELX. *Acta Crystallogr., Sect. A* **2008**, *64*, 112−122.
(55) Sheldrick, G. M. Crystal Structure Refinement with SHELXL. *Acta Crystallogr. C* **2015**, *71*, 3−8.
(56) Kent, A. D.; Vonolnar, S.; Gider, S.; Awschalom, D. D. Properties and Measurement of Scanning Tunneling Microscope Fabricated Ferromagnetic Particle Arrays. *J. Appl. Phys.* **1994**, *76* (10), 6656−6660.
(57) Brand, R. A. Improving the Validity of Hyperfine Field Distributions from Magnetic Alloys. Part I: Unpolarized Source. *Nucl. Instrum. Methods Phys. Res. A* **1987**, *B28*, 398−416.
(58) Brand, R. A. Improving the Validity of Hyperfine Field Distributions from Magnetic Alloys. Part II: Polarized Source and Spin Texture. *Nucl. Instrum. Methods Phys. Res.* **1987**, *B28*, 417−432.
(59) Bray, J. W.; Hart, H. R., Jr.; Interrante, L. V.; Jacobs, I. S.; Kasper, J. S.; Watkins, G. D.; Wee, S. H.; Bonner, J. C. Observation of a Spin-Peierls Transition in a Heisenberg Antiferromagnetic Linear-Chain System. *Phys. Rev. Lett.* **1975**, *35* (11), 744.
(60) Ding, L. J.; Yao, K. L.; Fua, H. H. Spin-Peierls Transition in Low-Dimensional Quantum Spin Systems: A Green's Function Approach. *Phys. Chem. Chem. Phys.* **2009**, *11*, 11415−11423.
(61) Rubín, J.; Badía-Romano, L.; Luis, F.; Mereacre, V.; Prodius, D.; Arauzo, A.; Bartolomé, F. Magnetic Chains of Fe3 Clusters in the {Fe3YO2} Butterfly Molecular Compound. *Dalton Trans.* **2020**, *49*, 2979−2988.
(62) Elhajal, M.; Canals, B.; Lacroix, C. Symmetry Breaking Due to Dzyaloshinsky-Moriya Interactions in the Kagomé Lattice. *Phys. Rev. B* **2002**, *66*, No. 014422.
(63) Evangelisti, M.; Bartolomé, J.; Luis, F. Experimental Evidence of Multiple Magnetic Relaxation Processes in Mn12 Acetate and Mn12-Cl Benzoate. *Solid State Commun.* **1999**, *112* (12), 687−691.
(64) Luis, F.; Bartolomé, J.; Fernández, J. F. Resonant Magnetic Quantum Tunneling through Thermally Activated States. *Phys. Rev. B* **1998**, *57*, 505.
(65) Fernández, J. F.; Alonso, J. J. Ordering of Dipolar Ising Crystals. *Phys. Rev. B* **2000**, *62*, 53.
(66) Fernández, J. F.; Luis, F.; Bartolomé, J. Time Dependent Specific Heat of a Magnetic Quantum Tunneling System. *Phys. Rev. Lett.* **1998**, *80*, 5659.
(67) Fernández, J. F.; Bartolomé, J.; Luis, F. Resonant Magnetic Quantum Tunneling through Thermally Activated States. *J. Appl. Phys.* **1998**, *83*, 6940−6942.
(68) Gómez-Coca, S.; Urtizberea, A.; Cremades, E.; Alonso, P. J.; Camón, A.; Ruiz, E.; Luis, F. Origin of Slow Magnetic Relaxation in Kramers Ions with Non-Uniaxial Anisotropy. *Nat. Commun.* **2014**, *5*, 4300.
(69) Filoti, G. *Basic Principles of Mössbauer Spectroscopy and Applicatiions in, NMR-MRI and Mössbauer Spectroscopies in Molecular Magnets*; Springer Verlag, 2007; pp 225−248.
(70) Renner, B.; Lehmann, G. Correlation of Angular and Bond Length Distortions in TO4 Units in Crystals. *Z. Kristallogr.* **1986**, *175* (1−2), 43−59.
(71) Liu, W.; Thorp, H. H. Bond Valence Sum Analysis of Metal-Ligand Bond Lengths in Metalloenzymes and Model Complexes. 2. Refined Distances and Other Enzymes. *Inorg. Chem.* **1993**, *32*, 4102−4105.
(72) Hatert, F.; Long, G. J.; Hautot, D.; Fransolet, A.-M.; Delwiche, J.; Hubin-Franskin, M. J.; Grandjean, F. A Structural, Magnetic, and Mössbauer Spectral Study of Several Na−Mn−Fe-Bearing Alluaudites. *Phys Chem Minerals* **2004**, *31*, 487−506.
(73) Brown, I. D. Recent Developments in the Methods and Applications of the Bond Valence Model. *Chem. Rev.* **2009**, *109*, 6858−6919.
(74) Bartolomé, J.; Filoti, G.; Kuncser, V.; Schinteie, G.; Mereacre, V.; Anson, C.; Powell, A.; Clerac, R.; Prodius, D.; Turta, C. Magnetostructural Correlations in the Tetra-Nuclear New Series of {Fe3LnO2} "Butterfly"Core Clusters: A Magnetic and Mössbauer Spectroscopic Study. *Phys. Rev. B* **2009**, *80*, No. 014430.
(75) Filoti, G.; Kuzmin, M. D.; Bartolomé, J. Mössbauer Study of the Hyperfine Interactions and Spin Dynamics in α-Iron(II) Phthalocyanine. *Phys. Rev. B* **2006**, *74*, No. 134420.
(76) Jaimes, E.; Iraldi, R.; González-Jiménez, F. Electric Field Gradient Sign Determination in Low Magnetic Fields Perpendicular to the Gamma Rays in 57Fe Mössbauer Spectroscopy. *Hyperfine Interact.* **1991**, *67*, 721−726.
(77) Reissner, M. *Mössbauer Spectroscopy in External Magnetic Fields*; Yoshida, Y.; Langouche, G., Eds.; Springer, 2021.